IEEE Access
Multidisciplinary ⋮ Rapid Review ⋮ Open Access Journal

Received February 14, 2022, accepted March 3, 2022, date of publication March 10, 2022, date of current version March 18, 2022.

Digital Object Identifier 10.1109/ACCESS.2022.3158647

Computationally Efficient Stator AC Winding Loss Analysis Model for Traction Motors Used in High-Speed Railway Electric Multiple Unit

PIL-WAN HAN[1], (Member, IEEE), UN-JAE SEO[2], (Member, IEEE), SARBAJIT PAUL[1], (Member, IEEE), AND JUNGHWAN CHANG[3], (Member, IEEE)

[1]Industry Applications Research Division, Electric Machines and Drives Research Center, Korea Electrotechnology Research Institute, Changwon 51543, South Korea
[2]Daegu Technical Center, Borgwarner Changnyeong LLC, Daegu 42713, South Korea
[3]Mechatronics System Research Laboratory, Electrical Engineering Department, Dong-A University, Busan 49315, South Korea

Corresponding author: Junghwan Chang (cjhwan@dau.ac.kr)

This work was supported by the Railway Vehicle Parts Development Project of Korea Agency for Infrastructure Technology Advancement (KAIA) funded by the Ministry of Land, Infrastructure and Transport of Korean Government under Grant 21RSCD-C160566-01.

ABSTRACT The aim of this proposed work is to develop a computationally efficient and accurate AC winding loss analysis model for the traction motors for use in high-speed railways (HSRs). The goal of the model is to be able to study AC winding loss under both sinusoidal and pulse width modulated (PWM) inverter voltage sources. The traction motor model considered for the proposed study is a form wound winding permanent magnet (PM) assisted synchronous reluctance motor (PMaSynRM). The traction motor uses an open slot with two-layer winding. First, a flux linkage table is built using finite element analysis (FEA) with sinusoidal current as the input. The machine model then includes the effect of the PWM inverter voltage source with the current controller. For the AC winding loss analysis, the fundamental component and the harmonics due to PWM are considered separately. To find the loss due to the fundamental component only, the vector potential of the slot region is mapped to the subconductors of the form wound winding and the eddy current distribution and the AC winding loss are calculated. The effect of the harmonics due to the PWM switching is then added in the post-processing stage by analytically evaluating the individual harmonic effect. The whole AC loss analysis model proposed in this work is computationally more efficient than the conventional FEA because the transient state of the system is removed. Moroover, the PWM voltage source effect is divided into the effects of the fundamental component and switching harmonics by combining the vector potentia mapping and post-processing analytical calculation.

INDEX TERMS AC winding loss, computationally efficient, distributed traction, electric multiple unit, finite element analysis, form wound winding, high-speed railway, PM-assisted synchronous reluctance motor, traction motor.

I. INTRODUCTION

To improve the ease of transportation and enable mass transit around the world, the demand for high-speed railways (HSR) has increased recently. For an HSR system, the use of electric traction is considered as the efficient option compared to the traditional traction methods like steam engines or diesel-electric engines [1]–[3]. The use of all-electric traction has its benefits like less environmental pollution, wide range of control with a quick start and stop. In an HSR traction system as shown in Figure 1(a), two different configurations are possible, namely, concentrated and distributed traction. In concentrated traction (CT)-HSR, the train uses two motorized cars at the two extreme ends of the train with passenger cars with no tractive force called trailer cars placed in the middle. Usually, the motorized car uses the megawatt-class large motor to develop the tractive force. Whereas the distributed traction (DT)-HSR uses kilowatt range motors and

The associate editor coordinating the review of this manuscript and approving it for publication was Ahmed A. Zaki Diab.

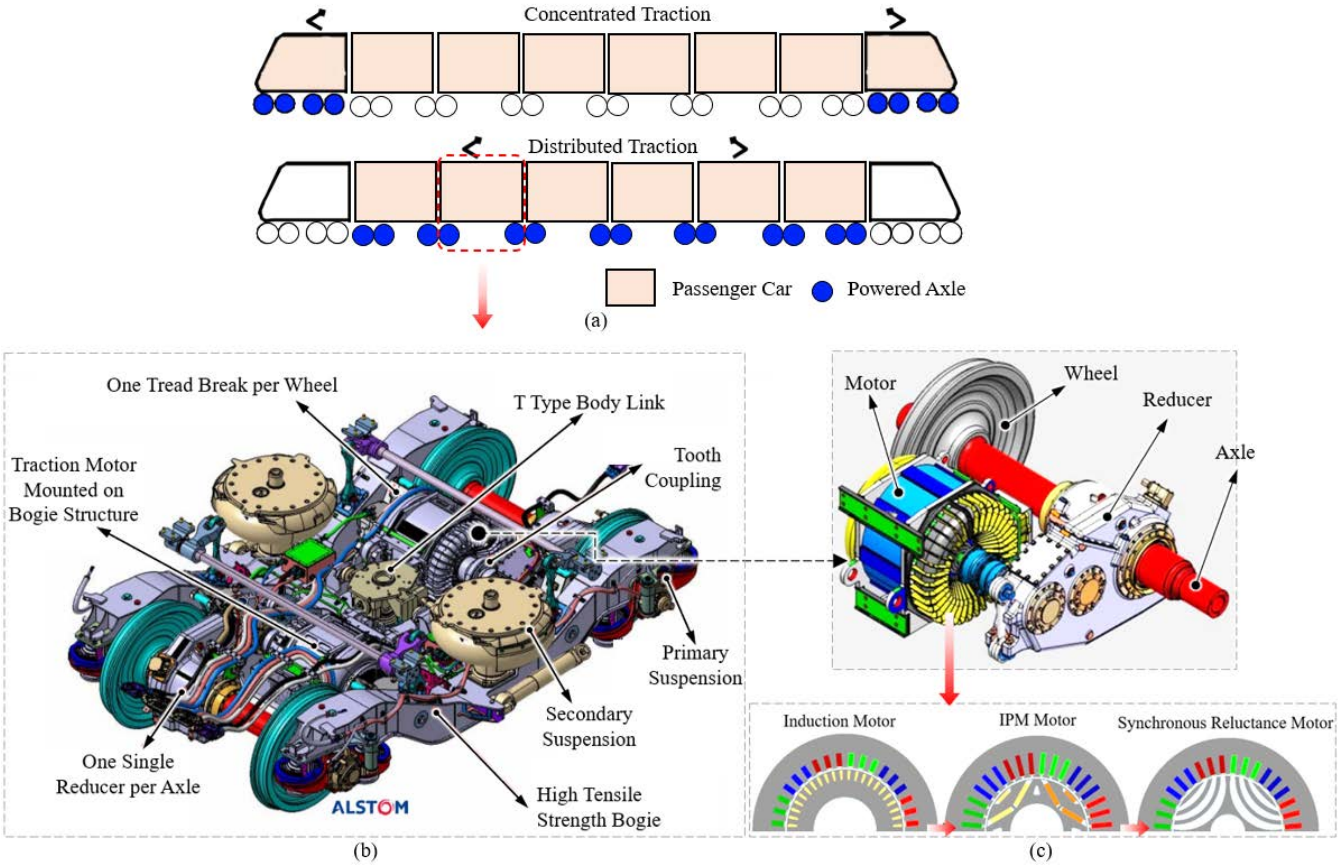

Factors	Concentrated Traction	Distributed Traction
Characteristics	Concentrated traction train configuration with motorized cars at the end with trailer cars with no tractive power in the middle	The tractive force is distributed among the cars in the middle equally with two trailer cars at the end
Rate of Consumption of Energy/Passenger	Higher	Lower
Train Weight	Higher	Lower
Axle Load/ unsprang mass	Disadvantage	Advantage

FIGURE 1. Different traction system for HSR: (a) concentrated and distributed tractions, (b) Alstom bogie for distributed traction HSR [4], (c) motor assembly with different motor topologies for distributed traction and (d) comparison between concentrated and distributed traction.

the tractive force is shared by a distributed set of motors installed with the wheel of the trailer cars as shown in Figure 1(a). The traction units can be called electric multiple units (EMUs). An example of the DT bogie developed by ALSTOM is shown in Figure 1(b) [4]. As shown in Figure 1(b), each bogie uses two electric motors and each motor is connected to the axle of two wheels on the side through a reducer.

When comparing a CT-HSR with the DT-HSR, the rate of energy consumption per passenger of a CT-HSR is higher than the DT-HSR. Furthermore, the train weight is also higher in the CT-HSR. For axle load per unsprung mass, the DT-HSR is advantageous over the CT-HSR. Considering the advantages of the system, the DT-HSR has gained wide attention recently [5].

For DT-HSR, as shown in Figure 1(c), different types of motors can be used. The selection of the motors is decided by the need for high performance and solutions with lower cost. The most widely used motor type in HSR traction is induction motors (IMs) [6]–[9]. The IMs are mechanically robust and have high overloading capabilities. Moreover, the IMs are low cost and can be connected in multiple drive configurations such as two motors connected in parallel in one drive termed as 1C2M configuration. In recent years, permanent magnet synchronous motors (PMSMs) have also found increased use in HSR applications [10]–[16]. In a PMSM, the electromagnetic torque is produced by the combination of the magnetic and the reluctance torques. The PMSMs have high efficiency and power density, however, need proper consideration in developing the mechanical design. Another

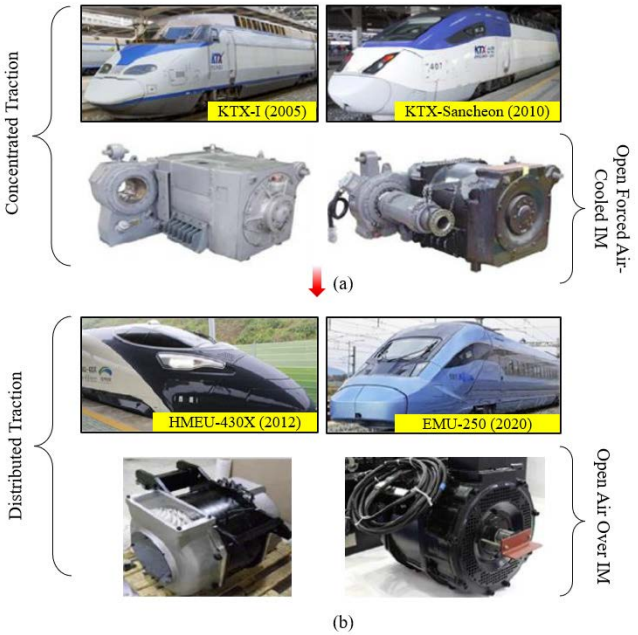

FIGURE 2. Existing HSR systems in south korea and their traction motors.

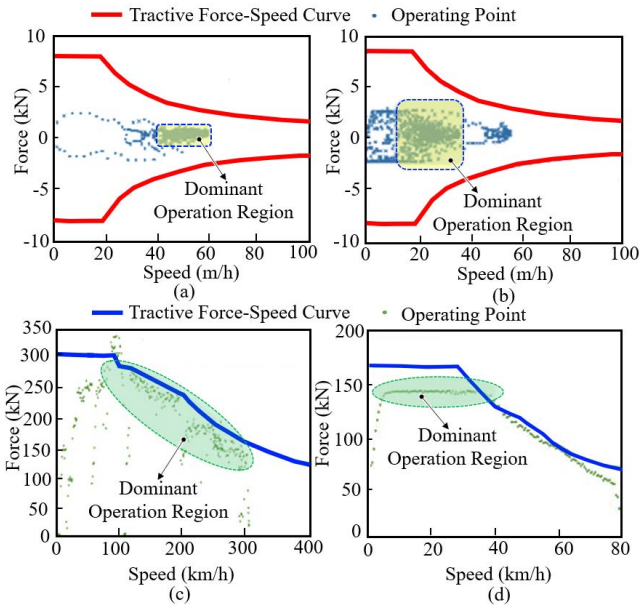

FIGURE 3. Different tractive force speed curves and operating ranges of the electric traction systems: (a) EV on FHDS, (b) EV on FUDS, (c) HSR and (d) LSR [48].

class of motor that has the potential for the HSR application is the synchronous reluctance motor (SynRM) in which the electromagnetic torque is produced by the variation of the reluctance [17]–[23]. Some SynRM models use PM to assist the reluctance torque called PM-assisted SynRM (PMaSynRM). However, no significant success has been reported so far. This is due to the performance constraint of the SynRM and the conservative attitude of the railway industry. Furthermore, the selection of the motor is also influenced by the cooling methods [24]–[26], the maximum allowed temperature of the insulation system [27]–[31], semi-conductor and power electronics drive technology [32]–[37], etc. An overall comparison of CT and DT-HSRs is shown in Fig. 1(d).

In South Korea, the first HSR was built considering the TGV model produced by France. The first generation HSR in South Korea used CT configuration as shown in Fig. 2 [38]. They are called the KTX-I and KTX-Sancheon HSR and the traction system uses a motor car with a high megawatt-class open forced air-cooled induction motor (IM) to generate the tractive force. In recent years, the South Korean HSR system has also used DT configuration in the HMEU-430X (2012) [39] series and the EMU-250 (2020) series, shown in Fig. 2(b) [40]. These DT-HSRs have used forced air-cooled IMs as traction motors.

In this proposed work, the use of a PMaSynRM has been considered for DT-HSR. To study the traction application of the PMaSynRM in DT-HSR, it is important to study the winding characteristics. The winding can be designed using circular (random wound stator slot) or rectangular conductors (form-wound stator slot) [41]. The use of rectangular conductors can improve the winding fill factor and are the straightforward option for high-voltage, high-power and high-speed motors. The form-wound stator windings are mechanically robust and better sealed against environmental threats [42]–[46]. Also, they are more durable than random wound windings. However, the use of form wound winding needs the stator to have open parallel slots. The drawbacks of open parallel slot design include the disturbances of the magnetic field in the airgap, torque pulsation, increase in noise and temperature [46]. Furthermore, the open parallel slot will result in AC resistance losses in the winding [47]. Therefore, in this proposed research, the aim is to develop an analysis tool to study the winding AC resistance losses for the form- wound winding for HSR. The use of commercial finite element analysis (FEA) software for the AC resistance loss can give satisfactory results however the design process is not computationally efficient. The proposed research aims to develop a computationally efficient AC winding loss analysis model that can predict the loss as accurately as the full FEA models with lower computational burden. The detailed step-by-step discussion on the steps needed to develop the analysis model is presented in the following sections.

II. INITIAL CONSIDERATION OF TRACTION MOTOR

To study the effect of the AC resistance losses on the performance of the traction motor for HSR, in this section detailed study of the operation characteristic and the topology selection of the traction motor for HSR is performed.

A. OPERATION CHARACTERISTICS

Usually, traction motors operate within the maximum torque/tractive force–speed curve. Figure 3 shows the tractive force-speed characteristics of different traction applications with frequent operating points of the vehicle highlighted in

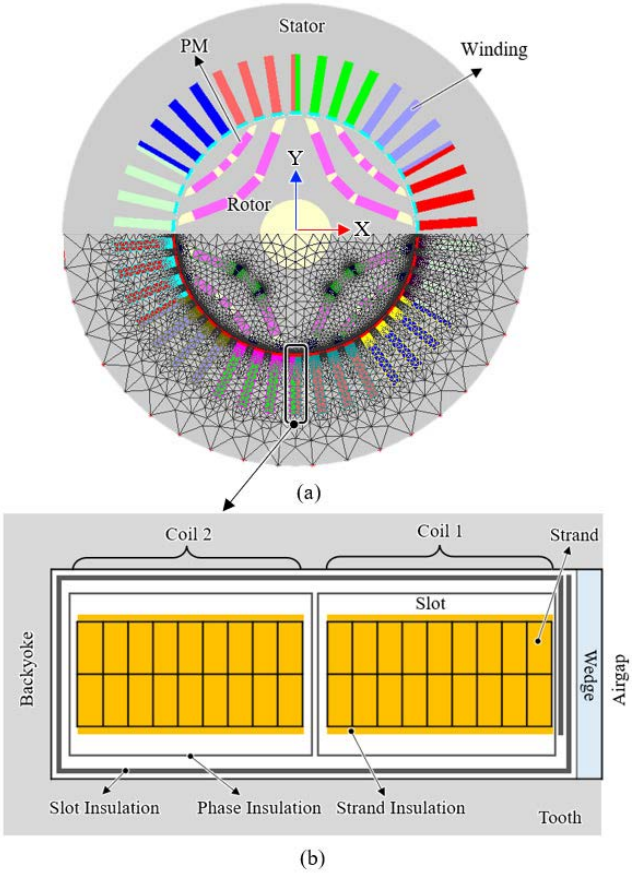

FIGURE 4. Schematic of the proposed HSR traction motor: (a) 2D-FEA model of the Proposed PMA-SynRM with (b) Tooth model.

dots. In the case of an electric vehicle (EV), the operation can be divided into Federal Highway Driving Schedule (FHDS) and Federal Urban Driving Schedule (HUDS), respectively. As shown in Figure 3(a) and (b), based on the driving schedule, the frequent operation points vary aggressively and hence the torque requirements, as well as other electromagnetic performances, will also change. When railway vehicles are considered, the distribution of frequent operation points for a HSR and its low-speed counterpart exhibit a notable difference, as illustrated in Figure 3(c) and(d) [48]. As a result, it is critical to consider the speed variation during dynamic operation while studying the performance of an electric motor for HSR applications.

B. TRACTION MOTOR TOPOLOGY

The HSR traction motor topology considered for this proposed research is a PMaSynRM as shown in Figure 4(a). The stator core is designed with 42 slots that accommodates a 4-pole fractional-slot distributed winding. The selection of the fractional slot distributed winding is inspired by its ability to reduce cogging torque. Furthermore, use of fractional slot winding has its inherent adventages like- the freedom of choice with respect to the number of slots, opportunity to reach sutable magnetic flux density with a given dimension, multiple alternative for short pitching and option for

TABLE 1. Ratings and specification of proposed PMaSynRM.

Parameters	Value
Rated Output Power (kW)	380
Base Speed (rpm)	2193
Maximum Speed (rpm)	4700
Base Frequency (Hz)	73.1
Maximum Frequency (Hz)	156.67
DC link Voltage (V)	3000
PWM Frequency (kHz)	2
Rated Current (A_{rms})	173.05
Frame Type	Totally Enclosed
Core Material	35PN230
PM Material	N40UH
Outer Diameter (mm)	520
Number turns per phase	42

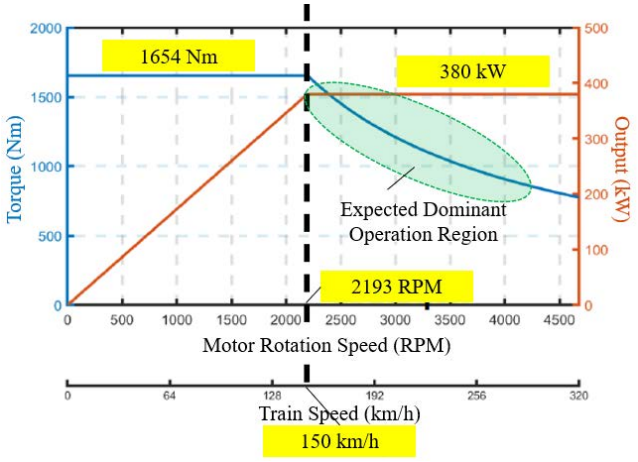

FIGURE 5. T-N curve for the proposed HSR traction motor.

segmented structures [49]. The basic design specifications of the proposed PMaSynRM are listed in Table 1 and the torque-speed characteristic is shown in Figure 5. As shown in Figure 5, the base speed for the proposed PMaSynRM is at 2193 rpm and the maximum speed is at 4700 rpm and it is expected that the proposed motor would frequently operate between the base and maximum speeds. Furthermore, the proposed motor is Totally Enclosed Air Over (TEAO) machine. Furthermore, the proposed PMaSynRM employs a form wound winding with a rectangular conductor with open parallel slots, as shown in Figure 4(b). As a result, it is expected that the AC resistance loss in the windings will vary as the operating points are varied, and the effect should be investigated. The analytical formulation of the AC winding loss for form wound winding will be developed first in the next section, and then a loss model will be proposed to analyze the AC winding loss more precisely with less computational burden.

III. ANALYSIS OF AC RESISTANCE LOSS

A. CALCULATION OF INCREASED AC LOSS FACTOR

It is well known that the apparent resistance of windings used in AC machines increases with frequency. In the case

of small-sized machines with few kW, the effect of AC resistance is ignored, however for large machines it is crucial to estimate the increase and its effect on the electromagnetic performance. Furthermore, when the machine is fed from an inverter, the AC resistance effect is amplified by the frequency of the PWM harmonics [47]. The causes of the AC resistance in an electric machine can be categorized into three effects namely, the *skin effect*, the *proximity effect* and the *circulating current* in the machine [49]. Their effect on the machine performance can be expressed using the resistance factor k_{R} as follows [49], [50]

$$k_{\mathrm{R}} = k_{\mathrm{s}} \cdot k_{\mathrm{p}} \cdot k_{\mathrm{c}} \tag{1a}$$

$$\frac{R_{\mathrm{ac}}}{R_{\mathrm{dc}}} = k_{\mathrm{R}} \tag{1b}$$

where, k_{s}, k_{p} and k_{c} are the factors attributable to the skin effect, proximity effect and the circulating currents, respectively. R_{ac} and R_{dc} are *ac* and *dc* winding resistances. For a slot width of b, the effective value of total current in a conductor I and the current density J, the Joule losses under *dc* and *ac* winding resistances for a single conductor can be given as

$$P_{\mathrm{dc}} = R_{\mathrm{dc}} I^2 = \frac{l}{\sigma_c b_c h_c} I^2 \tag{2a}$$

$$P_{\mathrm{ac}} = \frac{b_c l}{\sigma_c} \int_0^{h_c} J\, J^* \mathrm{d}y \tag{2b}$$

where, σ_c is the conductivity of the winding material, b_c is the width of the conductor, h_c is the real height of the conductor, l is the axial length and d y is considered for a current element. Using (1) and (2) the resistance factor for a single conductor can be given as

$$k_{\mathrm{R}} = \frac{R_{\mathrm{ac}}}{R_{\mathrm{dc}}} = \frac{P_{\mathrm{ac}}}{P_{\mathrm{dc}}} = \frac{b_c^2 h_c}{I^2} \int_0^{h_c} \underline{J}\, \underline{J}^* \mathrm{d}y \tag{3}$$

By solving the integration (3), the expression for the k_{R} has been proposed in [49]. For a slot with several conductors, the expression for k_{R} should be developed by considering the reduced conductor height, ξ. To derive the expression, as shown in Figure 6, a slot with multiple rectangular conductors is considered. As shown in Figure 6, each slot contains two series-connected conductors with nine parallel sub conductor on top of each other. The dimensions of different parameters are listed in Table 2. From [49], the expression for the reduced conductor height for the winding shown in Figure 6 can be written as

$$\xi = \alpha \cdot h_c = h_c \sqrt{\frac{1}{2} \omega \mu_0 \sigma_c \frac{b_c}{b}} \tag{4}$$

where, α is called the depth penetration, h_c is the height of the conductor, ω is the electric angular velocity, μ_0 is the permeability of vacuum, σ_c is the conductivity, b_{c} and b are

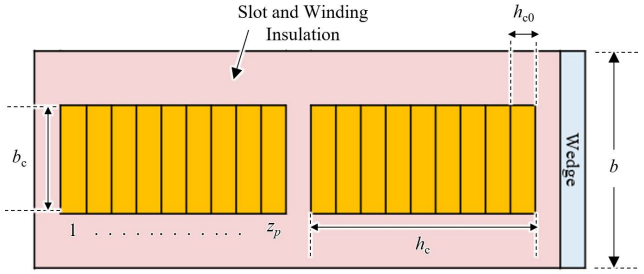

FIGURE 6. Dimension of open parallel slot with two layer form wound windings.

TABLE 2. Conductor dimension on each slot.

Parameters	Value
b (mm)	11.5
h_c (mm)	29.8
b_c (mm)	8.7
h_{c0} (mm)	3.31

the conductor and slot widths, respectively. Using the (4), the average resistance factor can be given as [49]

$$k_{\mathrm{R}} = \varphi(\xi) + \frac{z_t^2 - 1}{3} \psi(\xi) \tag{5}$$

with,

$$\varphi(\xi) = \xi \frac{\sinh 2\xi + \sin 2\xi}{\cosh 2\xi + \cos 2\xi}; \quad \psi(\xi) = 2\xi \frac{\sinh \xi - \sin \xi}{\cosh \xi + \cos \xi}$$

where, z_t is the number of conductor layers. From (4), it can be found that the reduced conductor height is dependent on the electric angular velocity and hence with the variation of motor operating speed, the value of the resistance factor will change. Moreover, the temperature change will also affect the resistance factor by changing the conductivity of the conductor material. Using (4) and (5), the resistance factor is calculated at different operating frequencies and temperatures for the proposed PMaSynRM and shown in Figure 7. For the calculation of k_{R} using (4)-(5), the effect of the end region is neglected as the skin effect in the end windings is usually negligible [49], [50]. In addition to having the average value of the k_{R}, it is important to check the variation of current density in each sub conductor and find the proximity effect between two conductors as shown in Figure 6. To check the current density variation, the help of electric circuit analysis is taken in the following subsection.

B. ANALYSIS OF CURRENT DENSITY DISTRIBUTION IN DOUBLE-LAYER FORM WOUND WINDING

To develop the electric circuit model and current distribution due to the AC resistance, the design is performed in two steps. First, a single layer conductor as shown in Figure 8(a) is considered. After analyzing the single layer conductor, the analysis is extended for the double layer winding.

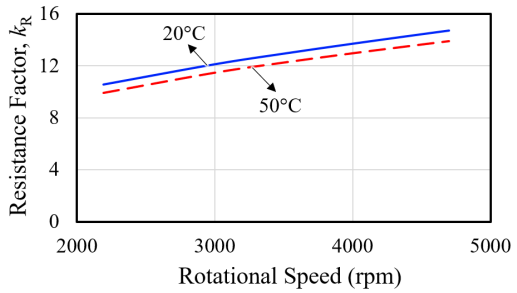

FIGURE 7. Variation of resistance factor, k_R with motor speed and temperature.

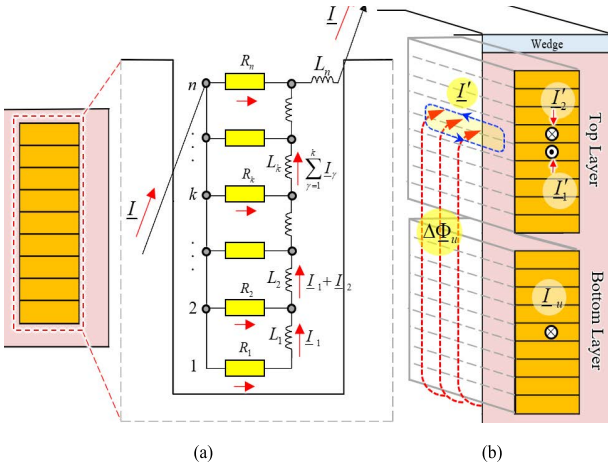

FIGURE 8. Equivalent circuit model analysis: (a) single layer conductor and (b) double layer conductors.

1) FOR SINGLE-LAYER CONDUCTOR

To develop the electric circuit model for the single-layer conductor, the following assumptions are made

1. The skin effect does not occur inside subconductors.
2. The current is flowing along the central line of the sub conductors.
3. The slot leakage only flows in the x-direction.

Based on the above considerations, in the steady-state, the voltage induced in the k^{th} subconductor by the slot leakage can be given as

$$\underline{E}_k = -j\omega\Delta\underline{\Phi}_k = R_k\underline{I}_k - R_{k+1}\underline{I}_{k+1} \tag{6}$$

where, $\Delta\underline{\Phi}_k$ is the leakage flux between the k^{th} and $(k+1)^{\text{th}}$ sub conductors, $\underline{I}_k$ and $\underline{I}_{k+1}$ are the currents in subconductors k and $k+1$, and ω is the angular velocity. The induced voltage creates a circulating current limited by the resistances R_k and R_{k+1}. Furthermore, the flux density B_k in the subconductor depends on the current linkage Θ_k calculated from the bottom of the slot to the subconductor k as follows

$$B_k = \mu_0\frac{\Theta_k}{b_k} = \mu_0\frac{1}{b_k}\sum_{\gamma=1}^{k} n_\gamma i_\gamma \tag{7}$$

where b_k is the width of the slot at the position of the kth subconductor and n_γ is the number of subconductors in the γth layer. The partial flux through the area limited by the paths of the currents I_k and I_{k+1} is

$$\Delta\Phi_k = B_k l h_k = \mu_0\frac{\Theta_k}{b_k} l h_k = \mu_0\frac{l h_k}{b_k}\sum_{\gamma=1}^{k} n_\gamma i_\gamma \tag{8}$$

where l is the axial staking length of the ferromagnetic core and h_k is the height of the kth subconductor. By substituting (8) into (6) and by employing phasors, we can obtain

$$\underline{E}_k = -j\omega\mu_0\frac{N l h_k}{b_k}\sum_{\gamma=1}^{k} n_\gamma i_\gamma = R_k\underline{I}_k - R_{k+1}\underline{I}_{k+1} \tag{9}$$

Next the expression for the current can be obtained as

$$\underline{I}_{k+1} = \frac{R_k}{R_{k+1}}\underline{I}_k + \frac{j\omega\mu_0}{R_{k+1}}\frac{l h_k}{b_k}\sum_{\gamma=1}^{k} n_\gamma i_\gamma \tag{10}$$

With the currents in the subconductors given, the total current in a conductor can be given by

$$\underline{I}_{\text{total}} = \sum_{k=1}^{n} I_k \tag{11}$$

As a circuit model, (6)-(11) can be represented by the parallel $R-L$ network as shown in Figure 8(a), where the values of R and L for each subconductor with surface area S_c can be given as

$$R_k = \frac{\rho l}{S_c}; \quad L_k = \mu_0\frac{l h_k}{b} \tag{12}$$

Equations (6)-(11) can be applicable for a single layer form wound winding. When the double layer is used as shown in Figure 8(b), the current flowing in a layer can affect the flux production on the other layer and should be considered during the electric circuit modeling.

2) FOR DOUBLE-LAYER CONDUCTOR

When the multiple layers share the same slot, the uppermost layer experiences the composed flux generated by itself and the lower layer. A schematic of the double layer case is shown in Figure 8(b). The presence of the proximity effect makes the circuit modeling of the double layer winding more complex.

In terms of current, the current in the subconductor k in the upper layer can be divided into two imaginary sections: the current of the subconductor k if it were alone in the slot: $\underline{I}_k$ (same as the single-layer case) and the current produced by the current in the underlying conductor: $\underline{I}'_k$. Thus the total current for subconductor k can be given as

$$\underline{I}''_k = \underline{I}_k + \underline{I}'_k \tag{13}$$

The total current in the lower conductor $\underline{I}_u$ creates a time-varying magnetic flux density in the upper conductor. The eddy current pattern created by this flux density has to be symmetrical with respect to the centerline of the upper conductor. The subconductors of the upper turn carry eddy currents that according to Lenz's law, attempt to cancel the

flux created by the lower turn current [49]. Therefore, the eddy current components at equal distances below and above the center of the conductor have to be equal in magnitude and opposite in directions

$$\underline{I}'_k = -\underline{I}'_{k-k+1} \tag{14}$$

From Figure 8(b), the current $\underline{I}'_1$ travels toward the observer, and the current $\underline{I}'_2$ run in the same direction as the sum of currents of the lower conductor. Now, the flux created by the total current $\underline{I}_u$ of the lower conductor induces a current $\underline{I}'_{k+1}$ in the upper conductor $k+1$. This current can be calculated in the $(k+1)^{\text{th}}$ subconductor analogously according to (10)

$$\underline{I}'_{k+1} = \frac{R_k}{R_{k+1}}\underline{I}'_k + \frac{j\omega\mu_0}{R_{k+1}}\frac{Nlh_k}{b_k}\left(\sum_{\gamma=1}^{k} n_\gamma \underline{I}'_\gamma + \underline{I}_u\right) \tag{15}$$

From Figure 8(b), with an even value of n, the subconductors $k = n/2$ and $k+1 = n/2+1$ constitute the center of the conductor and the current can be written as

$$\underline{I}'_{n/2+1} = -\underline{I}'_{n/2} = \frac{R_{n/2}}{R_{n/2+1}}\underline{I}'_{n/2} + \frac{j\omega\mu_0}{R_{n/2+1}}\frac{Nlh_{n/2}}{b_{n/2}}\underline{I}_m \tag{16}$$

where

$$\underline{I}_m = \left(\sum_{\gamma=1}^{n/2} n_\gamma \underline{I}'_\gamma + \underline{I}_u\right)$$

Based on (16), the currents in the other subcondcutors such as $n/2-1$ and $n/2$ are listed in Table 3. For the circuit design, the current excitation for each conductor is considered as sinusoidal, thus in real-life application, when an inverter is used, due to the PWM frequency, the current distribution in the conductors and the AC losses will vary. Consideration of PWM harmonics will make the circuit model and the analytical modeling complicated. Thus to address that issue, it is advisable to design the effect in FEA. However, for fast analysis, it is desired that the FEA model should be computationally efficient. In the next section, a novel AC winding loss analysis model will be developed to analyze the AC resistance losses in the form wound winding accurately with less computation burden.

IV. AC WINDING LOSS ANALYSIS FOR FORM WOUND WINDING

In traditional FEA modeling, winding modeling can be performed in two ways. In a straightforward way, the face regions can be developed and assigned as winding by coupled with the electric circuit. In this model, the mesh handling is easy as the winding regions with conductors and subcondctuors are not designed physically. Thus, the mesh can be coarse. On the other hand, when conductors and subconductors are designed physically as shown in Figure 9, the mesh number increases and hence the time to solve the model will also increase. The physical modeling of the conductors gives the designer the option to study the winding AC losses properly and current distribution due to the skin

TABLE 3. Current in different subcondcutors.

Subconductors	Value
$n/2$-1	$\underline{I}'_{n/2-1} = \frac{R_{n/2}}{R_{n/2-1}}\underline{I}'_{n/2} - \frac{j\omega\mu_0}{R_{n/2-1}}\frac{Nlh_{n/2-1}}{b_{n/2-1}}\left(\sum_{\gamma=1}^{n/2-1} n_\gamma \underline{I}'_\gamma + \underline{I}_u\right)$
$n/2$	$\underline{I}'_{n/2} = -\frac{j\omega\mu_0}{R_{n/2+1}}\frac{Nlh_{n/2}}{b_{n/2}}\left(\sum_{\gamma=1}^{n/2} n_\gamma \underline{I}'_\gamma + \underline{I}_u\right)$
$n/2$+1	$\underline{I}'_{n/2+1} = \frac{R_{n/2}}{R_{n/2+1}}\underline{I}'_{n/2} + \frac{j\omega\mu_0}{R_{n/2+1}}\frac{Nlh_{n/2}}{b_{n/2}}\left(\sum_{\gamma=1}^{n/2} n_\gamma \underline{I}'_\gamma + \underline{I}_u\right)$

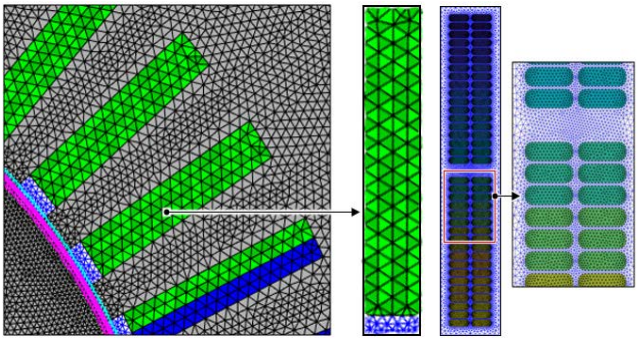

FIGURE 9. Mesh variation with physical design of winding.

and proximity effects can also be visualized. However, considering the computational inefficiency, the detailed modeling of the winding is usually avoided. In this section, the goal is to develop a novel computationally efficient AC winding loss analysis model for the proposed PMaSynRM where the detailed winding effect can be considered and the AC losses can be predicted accurately as those obtained from a full FEA model.

A. MODEL DEVELOPMENT AND MESH HANDLING FOR PMaSynRM MODELING

To develop the computationally efficient AC winding loss analysis model for the proposed PMaSynRM, the following three factors are considered

1) MDELING OF WIRE TRANSPOSITION

Wire transposition is used to reduce the circulating current loss in high voltage machines. The physical design of transposition is difficult and usually, the help of 3D modeling should be taken. For the proposed AC winding loss analysis model, the slot region is divided into the form wound conductors and their parallel subconductors and the transposition is done through electric circuit coupling on the specific subconductor regions as shown in Figure 10(a) from the positive to the negative coil sides.

2) EFFECT OF SOURCE

The performance of the FEA simulation varies with the selection of the electric source. Usually, sinusoidal or PWM voltage sources are used in the HSR traction motor analysis,

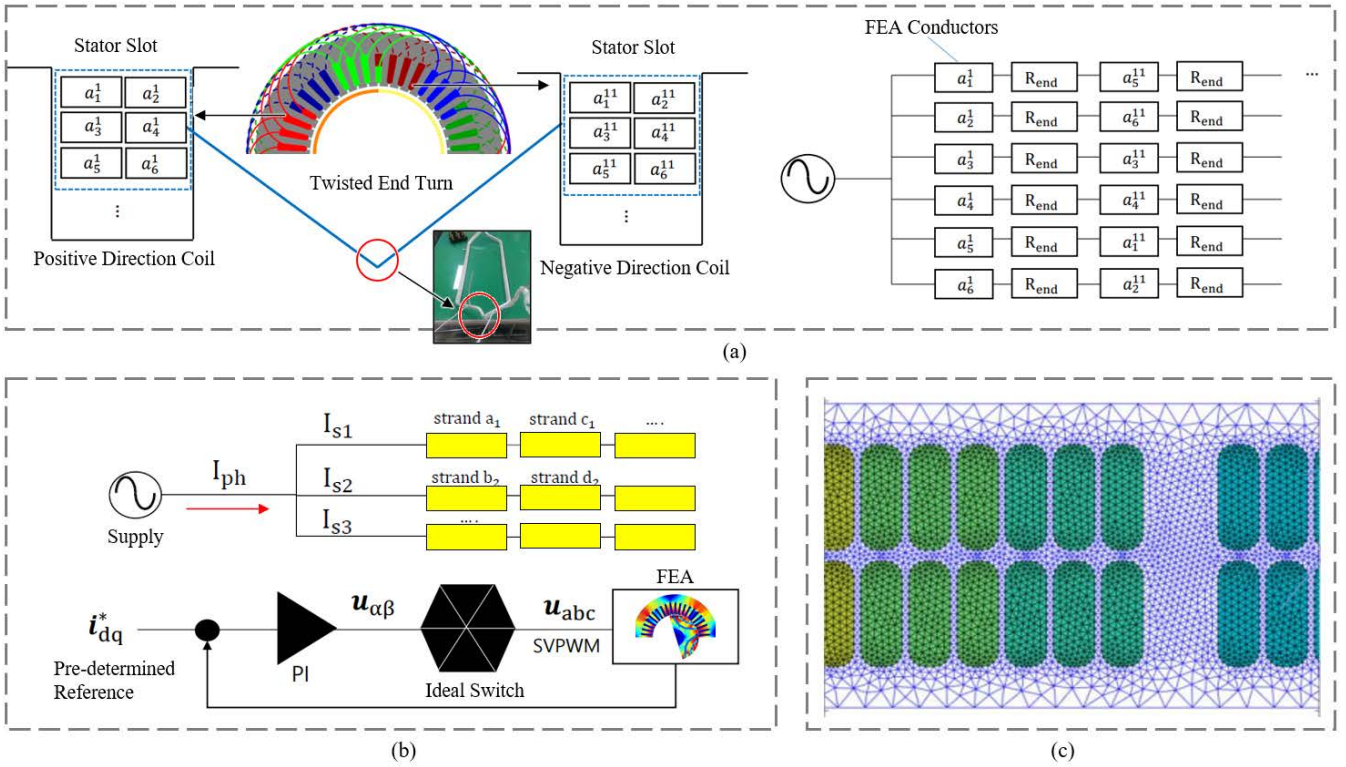

FIGURE 10. Design consideration: (a) Winding transposition, (b) selection of source and (c) meshing of slot region.

as shown in Figure 10(b). Based on the types of source, the simulation time varies as for the PWM inverter-based model, the time steps for simulation should be selected based on the switching frequency. Furthermore, the PWM voltage source model, as shown in Figure 10(b) needs a current controller and it results in the inclusion of the transient state in the simulation. The presence of the transient state will increase the simulation time and thus, this factor should be considered during the design stage of the AC winding loss analysis model.

3) MESHING OF STATOR SLOT

For the proposed PMaSynRM, there are 42 slots and each slot contains two layers *i.e* two form wound conductors which are also divided into parallel subcoductors. Thus to analyze the AC winding losses properly, if the physical modeling and mesh of each subcondctor are performed, it will result in a dense mesh as shown in Figure 10(c) with more than 600,000 meshes for the FEA model. This results in longer simulation time and computationally inefficient modeling. For the proposed work, a vector potential mapping method will be considered to make the whole analysis computationally efficient.

B. DEVELOPMENT OF THE AC WINDING LOSS ANALYSIS MODEL

The workflow for the proposed AC winding loss analysis model is shown in Figure 11. It can be divided into two main blocks, namely, the source simulation block and the AC winding loss analysis block. The model development can be explained using the following steps:

Step 1: In step 1, using the static FEA, the *dq* axes flux linkage table is developed. The flux linkage table contains the flux linkage values for different *d* and *q* axes currents. Flux linkage table stores the fundamental and harmonic components of the flux linkage. (Figure 12(a))

Step 2: Using the flux linkage table the electromagnetic performances such as the machine terminal voltage at different rotor speeds and torque can be calculated. The use of the flux linkage table rather than the full FEA reduces the computation time (Figure 12(b)). A Comparison of the terminal voltages obtained using the flux linkage table model with the full FEA at the base and maximum rpms are shown in Figure 13(a) and (b). Also, the comparison of the peak value of the terminal voltages at different speeds is shown in Figure 13(c). From Figure 13, it can be found that the flux linkage table model can accurately predict the electromagnetic performance of the proposed PMaSynRM.

Step 3: In step 3, the effect of the PWM inverter and current controller is considered. The PWM inverter model-based flux linkage table data includes the information on the *dq* axes current, flux linkage, current angle and current controller PI gains. When the Space Vector PWM (SVPWM) inverter and the current controller are added to the model, the time step will reduce due to the effect of the switching frequency and the current controller will introduce the transient state.

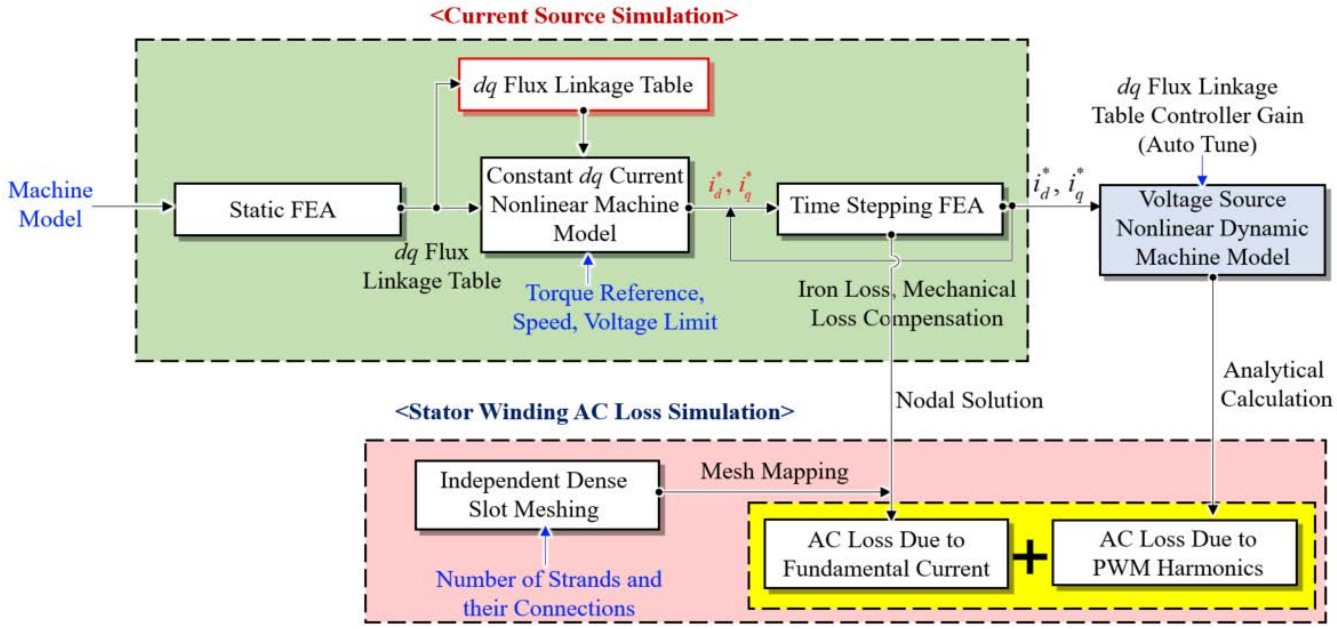

FIGURE 11. Workflow diagram of the AC winding loss analysis model.

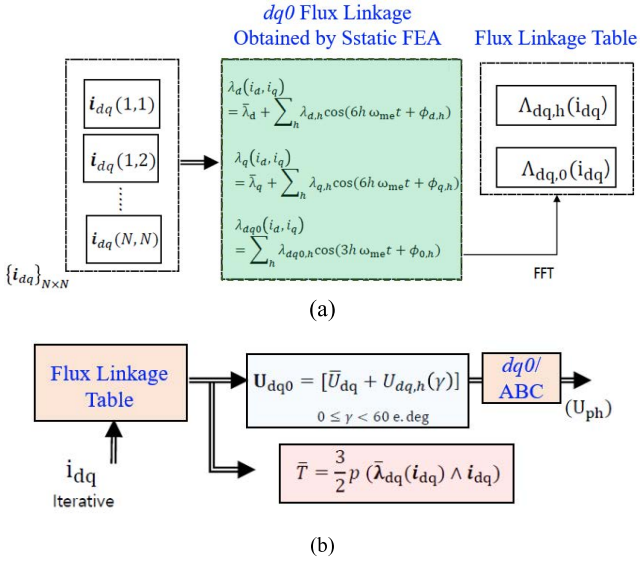

FIGURE 12. Steps to develop the flux linkage table.

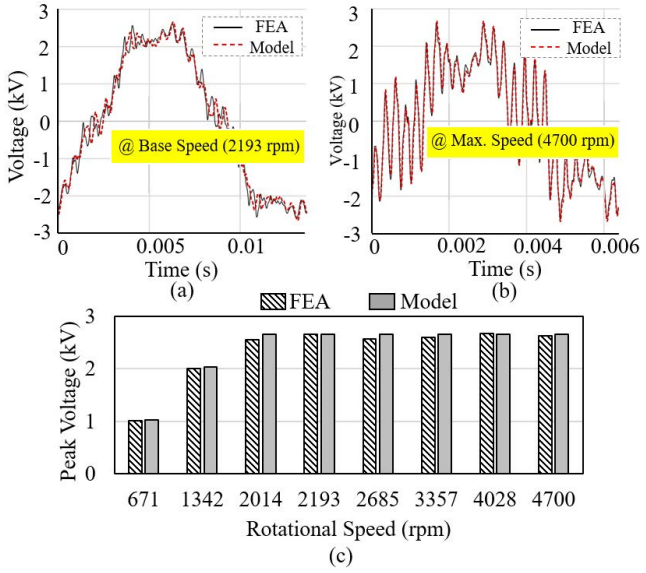

FIGURE 13. Comparison of the performance between the flux linkage table model and the full FEA model.

Figure 14 shows the PWM voltage, $i_d - i_q$ currents and three-phase currents. As it can be seen from Figure 14, at the beginning, the machine has a transient period and if it is included in the AC winding loss analysis, it will increase the simulation time and furthermore, the aim of the analysis is to check the loss at the steady-state. Therefore, while developing the flux linkage table, the data is filtered and the flux linkage table is made with the data when the machine reaches a steady state.

Step 4: Once the steady-state information such as the fundamental value of the voltage, current angle and PI controller information is obtained in step 3, the next step is to calculate the AC winding loss accurately and efficiently. To calculate the AC winding loss fast, the PWM voltage source effect has been divided into the effect of the sinusoidal fundamental component and the effect of the PWM harmonics. To calculate the effect of the sinusoidal fundamental component, the vector potential mapping at the slot region as shown in Figure 15(a) has been used. As shown in Figure 15(a), the vector potential value obtained from the sinusoidal FEA is mapped to the fine mesh nodes of the slot subconductors. Using the mapped vector potential value, the eddy current loss in the subconductors can be calculated as

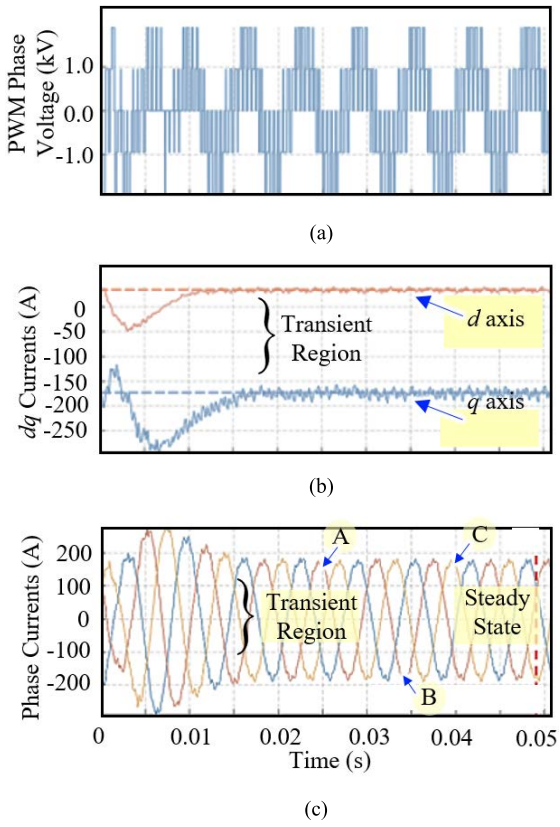

FIGURE 14. Effect of current controller and SVPWM on the machine voltage and current characteristics: (a) PWM voltage, (b) dq axes currents and (c) three phase instantaneous currents.

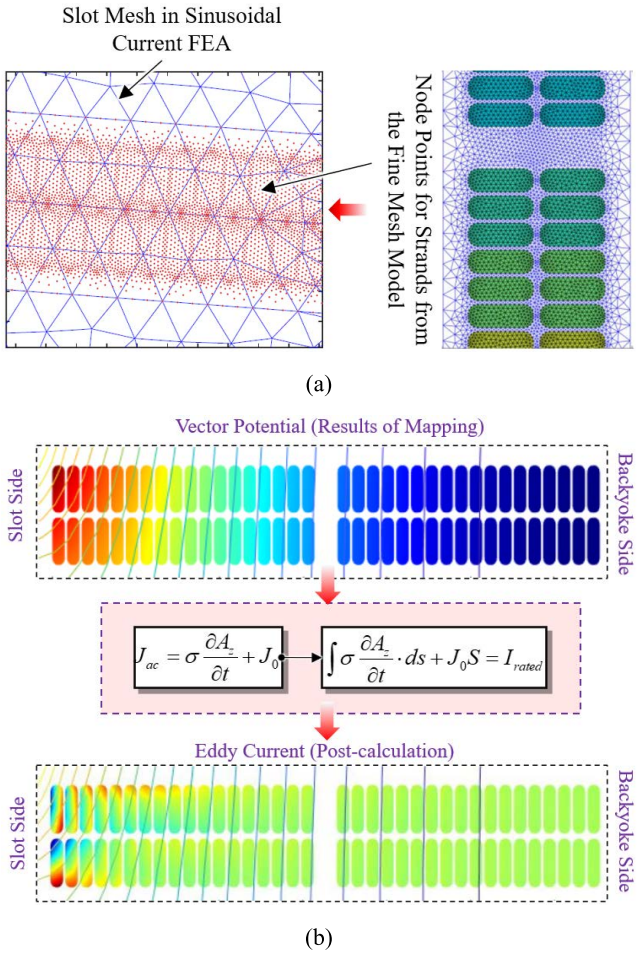

FIGURE 15. (a) Vector potential mapping by linking the potential to subconductor fine mesh nodes and (b) distribution of vector potential and the eddy current on the subconductors.

follows

$$\begin{cases} J_{ac} = \sigma \dfrac{\partial A_z}{\partial t} + J_0 \\ \displaystyle\int \sigma \frac{\partial A_z}{\partial t} \cdot ds + J_0 S = I_{rated} \end{cases} \tag{17}$$

where, J_{ac} is the eddy current in the subconductors, A_z is the vector potential in the z-direction, S is the surface area of each subconductor and the J_0 is a constant. The distribution of the vector potential under the sinusoidal fundamental component and the resultant eddy current on the subconductors are shown in Figure 15(b). It can be observed that the distribution of vector potential, as well as the eddy current, are different based on the location of the subconductors. Conductors closer to the slot opening have high eddy current variation. And hence, the AC winding losses will also increase near the slot opening. To calculate the effect of the PWM switching harmonics on the AC winding loss, the effect is added mathematically in the postprocessing stage to the sinusoidal simulation data using the mathematical model as follows [51]

$$\begin{cases} p_{ac/dc} = \dfrac{\sum_{k=2}^{\infty} I_k^2 p_{ac,k} + I_1^2 p_{ac,1}}{I_k^2} \\ P_{ac} = \dfrac{p_{ac/dc} \cdot l_{stk} + l_{end}}{l_{stk} + l_{end}} \displaystyle\sum_{k=1}^{\infty} I_k^2 R \end{cases} \tag{18}$$

where, k is the harmonic order and (18) considers the effect of PWM inverter source and resultant harmonics in the current waveform in the analysis of AC winding losses. The use of step 3 can successfully remove the effect of the system transient stage and mathematical modeling of the effect of the PWM harmonics on the AC winding loss in step 4 results in the reduction of the calculation, thus the whole simulation time for the AC winding loss model reduces. In the next section, the proposed AC winding loss model will be analyzed for different form wound winding types for the proposed PMaSynRM and its effectiveness will be compared with the full FEA model.

V. CALCULATION OF AC WINDING LOSS USING PROPOSED MODEL

The winding loss for the form wound windings for the PMaSynRM is determined in this section utilizing the AC winding loss analysis model described in the previous section. During the AC winding loss analysis using a PWM voltage source, the effect of the wedge types is also taken into account. The number of subconductors in each turn

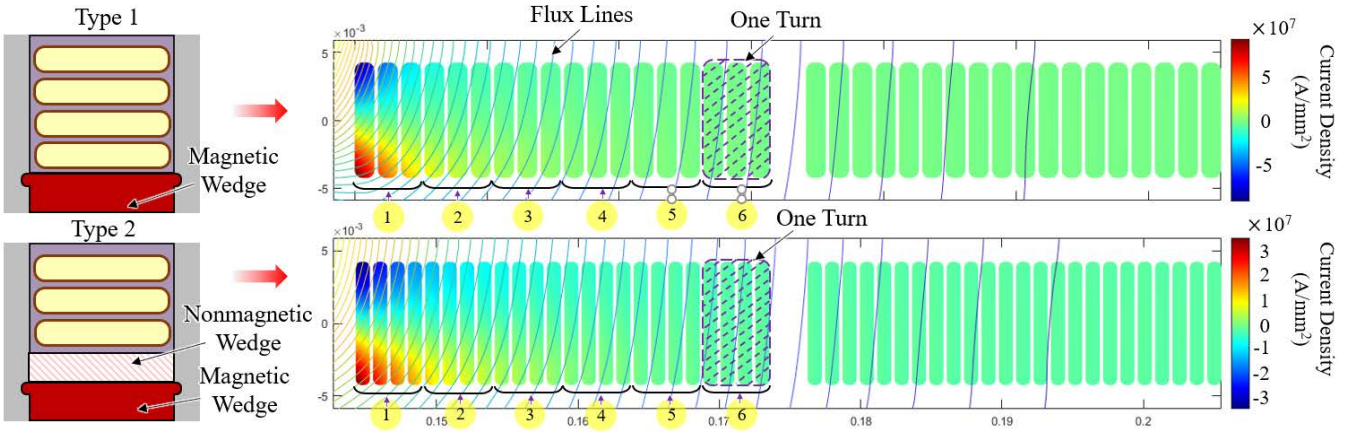

FIGURE 16. Distribution of current densities with types of wedges and subconductors under PWM inverter votlage source.

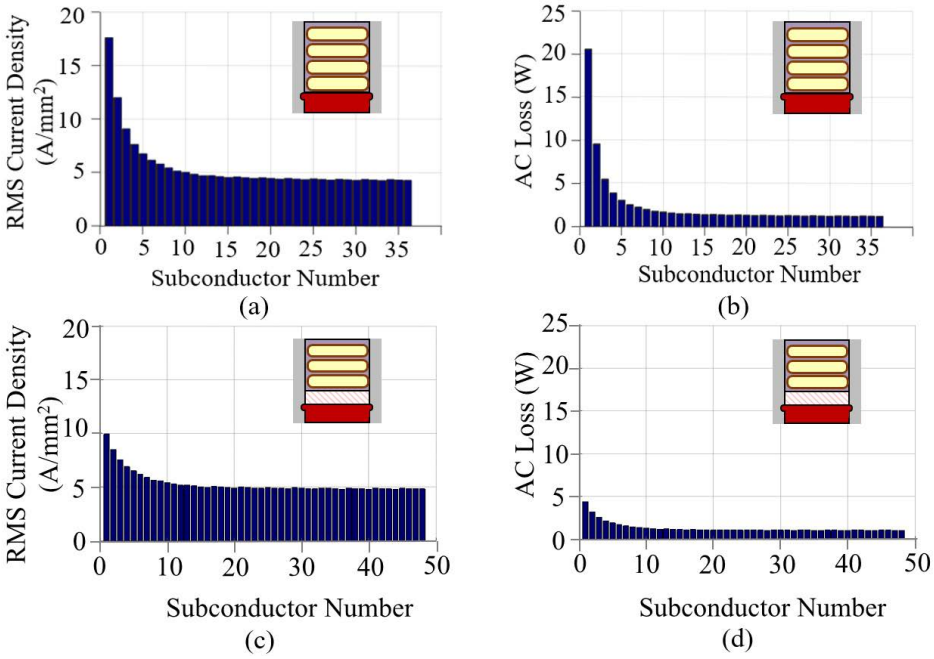

FIGURE 17. Distribution of RMS current density and AC winding losses (a) Type-1 RMS current density, (b) Type-1 AC loss, (c) Type-2 RMS current density and (d) Type-2 AC loss.

varies depending on the wedge type chosen, namely type 1 and type 2, as illustrated in Figure 16. For the type 1 and 2 models, 6 turns are used with each turn having three and four subconductors, respectively. Figure 16 depicts the current density distribution on each subconductor. Furthermore, Figure 17 displays the current density's RMS value as well as AC winding losses determined utilizing (18). Figures 16 and 17 show that, as compared to the type 1 wedge, the type 2 wedge is more effective at reducing AC winding losses. For example, the maximum subconductor AC winding loss is 21 W when type 1 wedge is used, whereas it reduces to 4.4 W when the type 2 wedge is considered. Furthermore, the total AC winding losses calculated using the proposed AC winding loss analysis model for type 1 and 2 models are shown in Figure 18. As shown in Figure 18, the average AC winding loss can be reduced by 8% when the type-2 wedge is used.

Furthermore, different types of subconductor models are analyzed for the PMaSynRM using the proposed AC winding loss analysis model. The calculation of the AC winding loss ratio and the AC winding losses using (18) is shown in Figure 19 (a) and (b). When compared with the conventional FEA model, it can be seen that the proposed model can predict the result under a similar level of accuracy. Thus, the proposed AC winding loss analysis model can provide a quick design tool for the engineers when analyzing the detailed AC winding losses and predict the performance of the HSR traction motor before manufacturing.

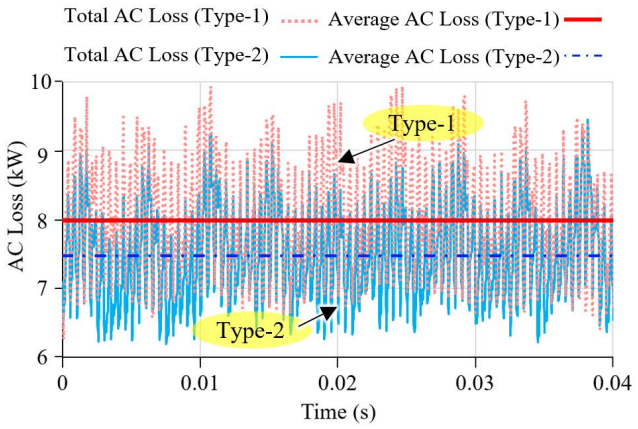

FIGURE 18. Total winding AC losses for type-1 and type-2 arrangements using the proposed AC winding loss analysis model.

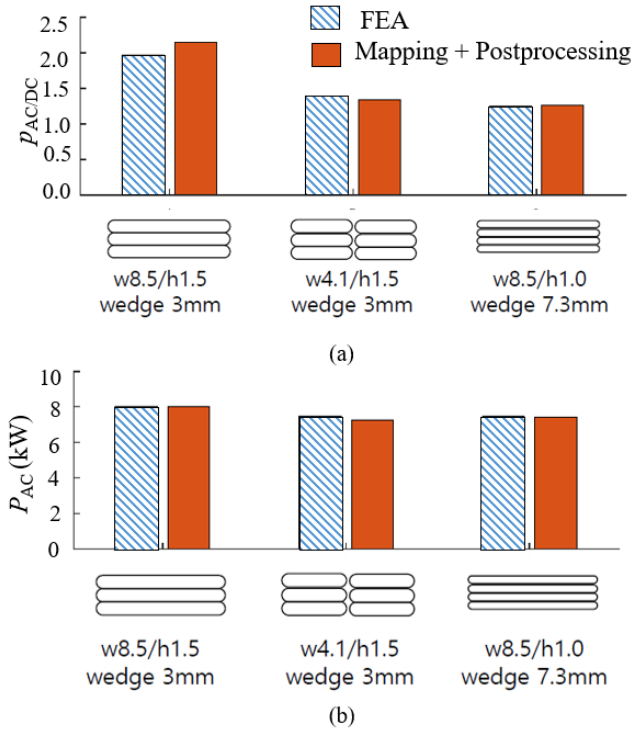

FIGURE 19. Comparison between conventional FEA and proposed AC winding loss analysis model for different subconductor types.

VI. CONCLUSION

A novel AC winding loss analysis model for a form wound winding permanent magnet (PM) assisted synchronous reluctance motor (PMaSynRM) for high-speed railway (HSR) distributed traction (DT) application has been proposed in this research. The contributions can be listed as follows-

1. The proposed AC winding loss analysis model aimed to eliminate the computation inefficiency of the conventional finite element analysis (FEA) model by introducing a vector potential mapping method combined with an analytical calculation of the switching harmonic losses produced by the pulse width modulated PWM) voltage sources.
2. Furthermore, to eliminate the effect of the transient state when current controllers are used, a flux linkage table was developed that can store only the steady-state information.
3. Removal of the transient state followed by the mapping of the vector potential of the fundamental component and its effect on AC winding loss and inclusion of the analytical calculation of switching harmonic losses makes the whole simulation process computationally fast compared to a conventional FEA.
4. This proposed model can be used as an effective tool in the initial design stage of the traction motors for the HSR application and different winding types and subconductor combinations can be considered and analyzed fast.

REFERENCES

[1] M. J. Hapeman, J. Long, and D. L. Plette, "Diesel electric locomotive propulsion systems—A look into the future," *IEEE Trans. Ind. Appl.*, vol. IA-22, no. 3, pp. 495–501, May 1986.
[2] A. Steimel, *Electric Traction Motive Power and Energy Supply, Basics and Practical Experience*. Munich, Germany: Oldenbourg Industrieverlag GmbH, 2003.
[3] R. J. Kemp, "Developments in electric traction," *Power Eng. J.*, vol. 3, no. 2, pp. 71–82, Mar. 1989.
[4] (2008). *The AGV, a Cutting-Edge Technology Integrator, INNOTRANS-BERLIN, Alsotom*. [Online]. Available: http://www.sze.hu/~szenasy/VILLVONT/TGV%2001_Presentation%20Alstom575km.pdf
[5] D. Ronanki, S. A. Singh, and S. S. Williamson, "Comprehensive topological overview of rolling stock architectures and recent trends in electric railway traction systems," *IEEE Trans. Transport. Electrific.*, vol. 3, no. 3, pp. 724–738, Sep. 2017.
[6] S. Nategh, A. Boglietti, Y. Liu, D. Barber, R. Brammer, D. Lindberg, and O. Aglen, "A review on different aspects of traction motor design for railway applications," *IEEE Trans. Ind. Appl.*, vol. 56, no. 3, pp. 2148–2157, May 2020.
[7] S. M. de Pancorbo, G. Ugalde, J. Poza, and A. Egea, "Comparative study between induction motor and synchronous reluctance motor for electrical railway traction applications," in *Proc. 5th Int. Electr. Drives Prod. Conf. (EDPC)*, Sep. 2015, pp. 1–5.
[8] A. Setiyoso, H. Hindersyah, A. Purwadi, and A. Rizqiawan, "Design of traction motor 180kW type SCIM for KRL (EMU) Jabodetabek re-powering project," in *Proc. Int. Conf. Electr. Eng. Comput. Sci. (ICEECS)*, Nov. 2014, pp. 341–344.
[9] S. Nategh, H. Zhang, O. Wallmark, A. Boglietti, T. Nassen, and M. Bazant, "Transient thermal modeling and analysis of railway traction motors," *IEEE Trans. Ind. Electron.*, vol. 66, no. 1, pp. 79–89, Jan. 2019.
[10] D. Yu, X. Y. Huang, Y. T. Fang, and J. Zhang, "Design and comparison of interior permanent magnet synchronous traction motors for high speed railway applications," in *Proc. IEEE Workshop Electr. Mach. Design, Control Diagnosis (WEMDCD)*, Apr. 2017, pp. 58–62.
[11] K. Yamazaki, S. Tamiya, K. Utsuno, K. Shima, T. Fukami, and M. Sato, "Rotor shape optimization for output maximization of permanent-magnet-assisted synchronous machines," *IEEE Trans. Ind. Appl.*, vol. 51, no. 4, pp. 3077–3085, Aug. 2015.
[12] H. Zheng, C. Wei, D. Sun, Y. Ren, L. Zeng, and R. Pei, "Rotor design of permanent magnet synchronous reluctance motors in rail traffic vehicle," in *Proc. 21st Int. Conf. Electr. Mach. Syst. (ICEMS)*, Oct. 2018, pp. 2762–2765.
[13] H. Douglas, F. Schmid, C. Roberts, and S. Hillmansen, "Evaluation of permanent magnet motor energy saving technology for different types of railways," in *Proc. IEEE Int. Conf. Intell. Rail Transp. (ICIRT)*, Aug. 2016, pp. 123–129.
[14] S. Kreuawan, F. Gillon, F. Moussouni, S. Brisset, and P. Brochet, "Optimal design of traction motor in railway propulsion system," in *Proc. Int. Aegean Conf. Electr. Mach. Power Electron.*, Sep. 2007, pp. 343–348.

[15] H. Jang, H. Kim, D.-W. Nam, W.-H. Kim, J. Lee, and C. Jin, "Investigation and analysis of novel skewing in a 140 kW traction motor of railway cars that accommodate limited inverter switching frequency and totally enclosed cooling system," *IEEE Access*, vol. 9, pp. 121405–121413, 2021.

[16] H.-C. Liu, H.-J. Lee, H.-S. Seol, S. Cho, J. Lee, and Y. J. Oh, "Optimal slot design of IPMSM in railway with independently rotating wheelsets," *IEEE Trans. Magn.*, vol. 55, no. 2, pp. 1–4, Feb. 2019.

[17] W. Zhao, F. Zhao, T. A. Lipo, and B.-I. Kwon, "Optimal design of a novel V-type interior permanent magnet motor with assisted barriers for the improvement of torque characteristics," *IEEE Trans. Magn.*, vol. 50, no. 11, pp. 1–4, Nov. 2014.

[18] A. Nobahari, A. Vahedi, and R. Nasiri-Zarandi, "A modified permanent magnet-assisted synchronous reluctance motor design for torque characteristics improvement," *IEEE Trans. Energy Convers.*, early access, Nov. 13, 2021, doi: 10.1109/TEC.2021.3127081.

[19] H. Douglas, F. Schmid, C. Roberts, and S. Hillmansen, "Evaluation of permanent magnet motor energy saving technology for different types of railways," in *Proc. IEEE Int. Conf. Intell. Rail Transp. (ICIRT)*, Aug. 2016, pp. 123–129.

[20] E. Trancho, E. Ibarra, A. Arias, I. Kortabarria, J. Jurgens, L. Marengo, A. Fricasse, and J. V. Gragger, "PM-assisted synchronous reluctance machine flux weakening control for EV and HEV applications," *IEEE Trans. Ind. Electron.*, vol. 65, no. 4, pp. 2986–2995, Apr. 2018.

[21] O. Korman, M. D. Nardo, M. Degano, and C. Gerada, "A novel flux barrier parametrization for synchronous reluctance machines," *IEEE Trans. Energy Convers.*, vol. 37, no. 1, pp. 675–684, Mar. 2022, doi: 10.1109/TEC.2021.3099628.

[22] J.-G. Lee and D.-K. Lim, "A stepwise optimal design applied to an interior permanent magnet synchronous motor for electric vehicle traction applications," *IEEE Access*, vol. 9, pp. 115090–115099, 2021.

[23] M. Murataliyev, M. Degano, and M. Galea, "A novel sizing approach for synchronous reluctance machines," *IEEE Trans. Ind. Electron.*, vol. 68, no. 3, pp. 2083–2095, Mar. 2021, doi: 10.1109/TIE.2020.2975461.

[24] *Electric Traction Rotating Electrical Machines for Rail and Road Vehicles—Part 2: Electronic Converter-Fed Alternating Current Motors*, document IEC 60349-2:2010, Oct. 2010.

[25] A. Acquaviva, O. Wallmark, E. A. Grunditz, S. T. Lundmark, and T. Thiringer, "Computationally efficient modeling of electrical machines with cooling jacket," *IEEE Trans. Transport. Electrific.*, vol. 5, no. 3, pp. 618–629, Sep. 2019.

[26] X. Liu, D. Gerada, Z. Xu, M. Corfield, C. Gerada, and H. Yu, "Effective thermal conductivity calculation and measurement of litz wire based on the porous metal materials structure," *IEEE Trans. Ind. Electron.*, vol. 67, no. 4, pp. 2667–2677, Apr. 2020.

[27] *IEEE Recommended Practice for Thermal Evaluation of Unsealed or Sealed Insulation Systems for AC Electric Machinery Employing Form Wound Pre-Insulated Stator Coils for Machines Rated 15 000 V and Below*, Standard 1776-2008, Feb. 2009.

[28] *Rotating Electrical Machines—Part 18-31: Functional Evaluation of Insulation Systems Test Procedures for Form-Wound Windings Thermal Evaluation and Classification of Insulation Systems Used in Rotating Machines*, document IEC 60034-18-31, Jun. 2012.

[29] L. Kung, U. Bikle, O. Popp, and R. Jakoby, "Improvement of the cooling performance of symmetrically self-ventilated induction machines in the 2–15 MW range," in *Proc. IEEE Int. Electr. Mach. Drives Conf. (IEMDC)*, Jun. 2001, pp. 673–680.

[30] V. Gavrilenko, A. Leonov, A. Bukharkin, S. Hlioui, and S. Lefebvre, "A method for endurance testing of enameled round and rectangular wires for motors controlled by SiC-based inverters," *IEEE Trans. Dielectr. Electr. Insul.*, vol. 28, no. 6, pp. 2091–2098, Dec. 2021.

[31] T. A. Huynh and M.-F. Hsieh, "Improvement of traction motor performance for electric vehicles using conductors with insulation of high thermal conductivity considering cooling methods," *IEEE Trans. Magn.*, vol. 57, no. 2, pp. 1–5, Feb. 2021.

[32] A. Rujas, V. M. Lopez, A. Garcia-Bediaga, A. Berasategi, and T. Nieva, "Influence of SiC technology in a railway traction DC-DC converter design evolution," in *Proc. IEEE Energy Convers. Congr. Expo. (ECCE)*, Oct. 2017, pp. 931–938.

[33] A. Marz, R. Horff, M. Helsper, and M.-M. Bakran, "Requirements to change from IGBT to full SiC modules in an on-board railway power supply," in *Proc. 17th Eur. Conf. Power Electron. Appl. (EPE ECCE-Eur.)*, Sep. 2015, pp. 1–10.

[34] L. Li, M. Wu, S. Wu, J. Li, and K. Song, "A three-phase to single-phase AC-DC-AC topology based on multi-converter in AC electric railway application," *IEEE Access*, vol. 7, pp. 111539–111558, 2019.

[35] L. Shen, J. Chen, Z. Jin, Z. Liu, D. Zhou, and C. Wu, "Resonating power decoupling using multifunctional bidirectional DC/DC converter in hybrid railway traction application," *IEEE Trans. Power Electron.*, vol. 37, no. 1, pp. 404–415, Jan. 2022.

[36] X. He, J. Peng, P. Han, Z. Liu, S. Gao, and P. Wang, "A novel advanced traction power supply system based on modular multilevel converter," *IEEE Access*, vol. 7, pp. 165018–165028, 2019.

[37] J. Fabre, P. Ladoux, H. Caron, A. Verdicchio, J.-M. Blaquiere, D. Flumian, and S. Sanchez, "Characterization and implementation of resonant isolated DC/DC converters for future MVdc railway electrification systems," *IEEE Trans. Transport. Electrific.*, vol. 7, no. 2, pp. 854–869, Jun. 2021.

[38] K.-S. Lee, J. K. Eom, J. Lee, and D. S. Moon, "The preliminary analysis of introducing 500 km/h high-speed rail in Korea," *Int. J. Railway*, vol. 6, no. 1, pp. 26–31, Mar. 2013.

[39] C.-S. Jeon, Y.-G. Kim, J.-H. Park, S.-W. Kim, and T.-W. Park, "A study on the dynamic behavior of the Korean next-generation high-speed train," *Proc. Inst. Mech. Eng., F, J. Rail Rapid Transit*, vol. 230, no. 4, pp. 1053–1065, May 2016.

[40] *Development of Driving Control Technology for Permanent Magnet Synchronous Motor for 380kW High-Speed Rail*, Under Ministry of Science and ICT, South Korea, 2019. [Online]. Available: https://www.ntis.go.kr/project/pjtInfo.do?pjtId=1711078634&pageCode=TH_TOTAL_PJT_DTL

[41] Y. Zhao, D. Li, T. Pei, and R. Qu, "Overview of the rectangular wire windings AC electrical machine," *CES Trans. Electr. Mach. Syst.*, vol. 3, no. 2, pp. 160–169, Jun. 2019.

[42] H. Barr, A. Bonnett, and C. Yung, "Understanding the design of stators and rotors of squirrel cage induction motors," in *Proc. 55th IEEE Petroleum Chem. Ind. Tech. Conf.*, Sep. 2008, pp. 1–11.

[43] G. L. Olson, *Bar-Wound Versus Wire-Wound Alternators*, document Power topic # 9013, 2010.

[44] A. Mesrobian and J. H. Holdrege, "Random wound versus form wound on low voltage synchronous generators," in *Proc. 37th Annu. Conf. Petroleum Chem. Ind.*, Sep. 1990, pp. 185–190.

[45] J. Haldemann, "Transpositions in stator bars of large turbogenerators," *IEEE Trans. Energy Convers.*, vol. 19, no. 3, pp. 553–560, Sep. 2004.

[46] P. Lindh, H. Jussila, J. Pyrhönen, A. Parviainen, and M. Niemelä, "Concentrated wound PM motors with semi-closed slots and with open slots," *Int. Rev. Electr. Eng.*, vol. 5, no. 2, pp. 491–497, 2010.

[47] M. J. Islam, H. V. Khang, A.-K. Repo, and A. Arkkio, "Eddy-current loss and temperature rise in the form-wound stator winding of an inverter-fed cage induction motor," *IEEE Trans. Magn.*, vol. 46, no. 8, pp. 3413–3416, Aug. 2010.

[48] H.-W. Lee, C.-B. Park, and B.-S. Lee, "Performance comparison of the railway traction IPM motors between concentrated winding and distributed winding," in *Proc. IEEE Transp. Electrific. Conf. Expo. (ITEC)*, Jun. 2012, pp. 1–4.

[49] J. Pyrhonen, T. Jokinen, and V. Hrabovcova, *Design of Rotating Electrical Machines*, 2nd ed. Hoboken, NJ, USA: Wiley, 2013.

[50] A. Tessarolo, C. Ciriani, N. Elloumi, M. Mezzarobba, and A. Masmoudi, "Fast computation method for stator winding skin-effect additional losses in synchronous machines with open slots and arbitrary rotor geometry," *IEEE Trans. Energy Convers.*, vol. 36, no. 2, pp. 1156–1168, Jun. 2021.

[51] C. Carstensen, "Eddy currents in windings of switched reluctance machines," Ph.D. dissertation, Dept. Elect. Eng. Inf. Technol., RWTH Aachen, Aachen, Germany, 2008.

PIL-WAN HAN (Member, IEEE) received the B.S., M.S., and Ph.D. degrees in electrical engineering from Hanyang University, Seoul, South Korea, in 1998, 2000, and 2013, respectively.

From 2000 to 2005, he was with LG Electronics. Since 2005, he has been with the Korea Electrotechnology Research Institute, Changwon, South Korea, where he is currently a Principal Researcher with the Electric Machines and Drives Research Center. His research interest includes the design and analysis of high efficiency electric machine for traction and industry applications.

UN-JAE SEO (Member, IEEE) received the B.S. degree in electrical engineering from Dong-A University, Busan, South Korea, in 2010, the M.S. degree in energy conversion from the University of Science and Technology, Daejeon, South Korea, in 2013, and the Ph.D. degree in electrical engineering from RWTH Aachen University, Aachen, Germany, in 2018.

From 2018 to 2021, he was a Postdoctoral Researcher with the Industrial Applications Research Division, Electric Machines and Drives Research Center, South Korea. Since 2021, he has been a Senior Engineer with the Technical Center Borgwaner, Daegu, South Korea.

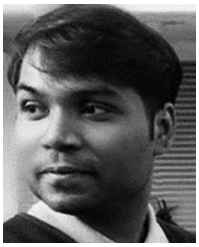

SARBAJIT PAUL (Member, IEEE) received the M.Sc. and Ph.D. degrees in electrical machine and power electronics, electrical engineering from the Mechatronics System Research Laboratory (MSRL), Department of Electrical Engineering, Dong-A University, Busan, South Korea, in 2016 and 2022, respectively.

From 2014 to 2016, he was a Korean Government Research Scholar, under the sponsorship of the National Institute of International Education (NIIED), Ministry of Education, South Korea. He is currently working at the Industry Application Research Division, Electric Machine and Drive System Research Center, Korea Electrotechnology Research Institute (KERI). His current research interests include motor design, electromechanical energy conversion, sensors, and actuators. He is a member of the IEEE Industrial Electronics Society's Technical Committee on Control, Robotics and Mechatronics. He is also a member of the Electrical Machinery and Energy Conversion Systems Society of the Korean Institute of Electrical Engineers (KIEE). He was a recipient of the Australia Award Endeavour Research Fellowship from 2017 to 2018 to perform part of his research at the University of New South Wales, where he developed different winding designs for printed circuit board micromachines. He was a recipient of the 2016 Travel Grant Award by the IEEE Instrumentation and Measurement Society, the 2017 Best Research Paper Award by the IEEE Region 10 (Asia-Pacific), and five Best Research Paper Awards from KIEE.

JUNGHWAN CHANG (Member, IEEE) received the B.S. and M.S. degrees in electrical engineering and the Ph.D. degree in precision mechanical engineering from Hanyang University, Seoul, South Korea, in 1994, 1997, and 2001, respectively.

From 2001 to 2002, he was with the Institute of Brain Korea 21, Hanyang University, where he developed micro drive and high-speed spindle motor. From 2002 to 2003, he was a Research Fellow with the University of California at Berkeley, Berkeley, CA, USA, where he analyzed and developed electrically controlled engine valve system. From 2003 to 2009, he was a Technical Leader with the Korea Electrotechnology Research Institute, South Korea, where he was involved in the developments of special purpose machines. Since 2009, he has been a Professor with the Department of Electrical Engineering, Dong-A University, Busan, South Korea. His current research interests include the design and analysis of electromechanical systems, such as electrically driven machine tools, and magnetic gear.

Dr. Chang is a member of the Korea Institute of Electrical Engineers, South Korea. He was a Steering Committee Member and the Technical Program Chair in different conferences, such as ICEMS 2013, IEEE ITEC Asia-Pacific 2016, COMPUMAG 2017, and ICEMS 2018. He is a Reviewer of the IEEE TRANSACTIONS ON MAGNETICS, the IEEE TRANSACTIONS ON INDUSTRIAL ELECTRONICS, the IEEE TRANSACTIONS ON INDUSTRIAL APPLICATION, and the IEEE/ASME TRANSACTIONS ON MECHATRONICS.